Theory of the hysteresis loop in ferromagnets

Igor F. Lyuksyutov*
Department of Physics, Texas A&M University, College Station, Texas 77843-4242

Thomas Nattermann
Institut für Theoretische Physik, Universität zu Köln, 50937, Köln, Germany
and Ecole Normale Superieure, Laboratoire de Physique Theorique, 24 rue Lhomond 75231, Paris Cedex 05, France

Valery Pokrovsky
Department of Physics, Texas A&M University, College Station, Texas 77843-4242
and Landau Institute for Theoretical Physics, Moscow, Russia
(Received 12 January 1998)

We consider three mechanisms of hysteresis phenomena in alternating magnetic field: the domain-wall motion in a random medium, the nucleation, and the retardation of magnetization due to slow (critical) fluctuations. We construct a quantitative theory for all these processes. The hysteresis is characterized by two dynamic threshold fields, a coercive field and the so-called reversal field. Their ratios to the static threshold field is shown to be a function of two dimensionless variables constituted from the frequency and amplitude of the ac field as well as from some characteristics of the magnet. The area and the shape of the hysteresis loop are found. We consider different limiting cases in which power dependencies are valid. Numerical simulations show the domain-wall formation and propagation and confirm the main theoretical predictions. Theory is compared with available experimental data. [S0163-1829(98)06545-X]

I. INTRODUCTION

The hysteresis loop (HL) was first studied more than a century ago.[1] However, the understanding of this process in thin magnetic films as well as in bulk magnets is still rather poor. Many efforts have been devoted recently to prediction (see Refs. 2–6) and experimental verification (see Refs. 7–9) of the scaling behavior of the hysteresis loop area (HLA) as a function of the applied magnetic-field frequency and amplitude for thin magnetic films (for a brief review of HLA scaling results, see Ref. 9). The scaling behavior of the HLA was first reported in the pioneer work[1] for three-dimensional (3D) magnets. While there exists an extended literature on the hysteresis of 3D magnets, the properties of HL in 2D systems are much less known. There are only few articles devoted to the HL in ultrathin ferromagnetic films,[10,11,7–9] though the hysteresis effects have been found as a side effect in many others (see, for example, Refs. 12 and 13). Critical exponents found in the experiments with thin films vary dramatically for different materials (see, e.g., Refs. 7–9) and probably for different regimes. Different authors disagree with each other (see the already cited articles[7–9]) and also disagree with numerical simulations.[2]

Several years ago mean-field-type models with single[10] or many[11] relaxation times have been applied to analyze experimental data. The authors of Refs. 10 and 11 assumed that the HL was controlled by the nucleation process. These authors predicted the logarithmic dependence of the coercive field h_c on the rate of the applied magnetic field $\dot{h}$. In a recent experiment[9] it was found that the HLA depends on the frequency of the applied field as a power with a small exponent ($\sim 0.03-0.06$) or, possibly, there is a logarithmic dependence. However, in the framework of the same approach the HLA must behave also as logarithm of h with the same coefficient (exponent). This dependence has never been observed in the experiment. Therefore, we propose a new analysis of such a HL in this paper.

The purpose of this paper is to formulate a rather general approach to magnetization reversal mechanisms and to indicate several important measurable characteristics of the HL besides the HLA. We will see that these characteristics are governed by two dimensionless parameters combined from the field frequency ω, its amplitude h_0, and characteristics of the magnetic material. Everywhere in what follows we assume that the external field varies harmonically in time, $h(t)=h_0\sin\omega t$.

The hysteresis behavior may have various origins. It can be mediated by the nucleation process, by the domain-wall (DW) propagation or simply by retardation of the magnetization due to fluctuations. We consider all these mechanisms and establish conditions at which one of them is dominant.

Defects play an important role in the DW propagation. They create a finite threshold value h_p of static magnetic field necessary for the DW depinning. The threshold field h_{t1} in the dynamical problem can differ substantially from h_p. We find that in a medium with defects the moving DW, passing rare extended defects, may form bubbles of reversed spins. These bubbles play an important role as prepared nuclei in the next half-cycle of the magnetization reversal.

In this paper we consider magnets of the Ising (uniaxial) symmetry. Their properties may be very different depending on the strength of the anisotropy. In the experimentally studied films the anisotropy was very weak. In this case the domain-wall width is large in comparison to the lattice constant. On the contrary, in the original Ising model the anisotropy is assumed to be large and DW width l is simply the

lattice constant. However, these different models become equivalent after a simple rescaling: the DW width should be accepted as a new elementary (cutoff) length. It means that we consider a spin cluster of the linear size l as a new elementary spin. This approach allows us to apply the Ising model supplied with the Glauber dynamics for numerical simulations.

Peculiarities of the two-dimensional situation are much higher mobility of the DW as well as much stronger fluctuations. This makes the experimental situations as well as the theoretical description much more diverse than those for a 3D magnet.

This article is organized as follows. In Secs. II and III we consider the individual DW motion. Equation of motion is formulated and justified in Sec. II. It is solved in Sec. III. In the same section we introduce characteristic fields h_{t1}, h_{t2}, h_c, h_r, the HLA $\mathcal{A}$, find the scaling arguments, and analyze several limiting regimes in which simple power scaling is valid. In Sec. IV the process of the bubble formation is studied. Section V is devoted to the HL controlled by the nucleation process. The HL driven by strong magnetization fluctuations, especially near the Curie point, is considered in Sec. VI. Numerical simulations of the HL and the domain structures for the 2D Ising model with Glauber dynamics that supports results obtained in Secs. III and IV are presented in Sec. VII. In Sec. VIII we summarize our results and compare them to the experimental data. In the rest of this article we use the notation h for magnetic field, m for magnetization, and M for the total magnetic moment of a magnet.

II. DOMAIN-WALL MOTION IN A RANDOM MEDIUM

As we already mentioned in the Introduction, our starting point is an impure ferromagnet with either weak or strong Ising anisotropy. The soft spin version of the system is then given by a ϕ^4 model with a bare domain-wall width $l \gg a$, where a denotes the original lattice spacing. The imperfections in the model may be in principle either of random bond (i.e., random T_c) or random-field type. We will argue below that in the region we are mainly interested in, namely, above the depinning threshold, both types of impurities act essentially as random-field impurities.

As it was shown by Bausch *et al.*[15] (see also Refs. 16 and 17), equation of motion for a domain wall without overhangs can be written in the following way:

$$\frac{1}{\gamma\sqrt{g}}\frac{\partial Z}{\partial t} = \Gamma\nabla\cdot(g^{-1/2}\nabla Z) + h + \eta(\mathbf{x}, Z) \tag{1}$$

where $Z(\mathbf{x},t)$ denotes the interface position and $g = 1 + (\nabla Z)^2$. γ and Γ are the domain-wall mobility and stiffness, respectively. $h = \mu_B H M$, where H is the external magnetic field and M is the magnetization. Finally η denotes the random force generated by the impurities.

For broad domain walls $\Gamma \approx J/(a^{D-1}l)$, where D denotes the dimensionality of the wall. For narrow walls Γ depends in general on J, T, and the disorder strength in a complicated way.[18]

The random fields $\eta[\mathbf{r} = (\mathbf{x}, Z)]$ generated by imperfections is assumed to be Gaussian distributed and short-range correlated with $\overline{\eta(\mathbf{r})} = 0$ and

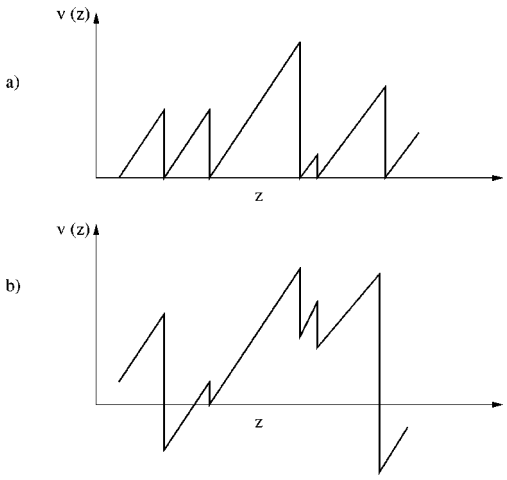

FIG. 1. Schematic picture of the ratcheted potential in the random-bond (a) and random field (b) cases.

$$\overline{\eta(\mathbf{r})\,\eta(\mathbf{r}')} = \eta^2 l^{D+1}\delta_l(\mathbf{r}-\mathbf{r}'). \tag{2}$$

Here $\delta_l(\mathbf{r})$ denotes a delta function smeared out over a distance l. As was first argued by Narayan and Fisher,[14] in the region above the depinning threshold random-bond and random-field impurities act in a similar way. This can be seen most easily from an example of two ratcheted potential (see Fig. 1), one for random-bond and another for random-field impurities. Although the potential $V(Z) = \int_0^Z \eta(\mathbf{x}, Z')dZ'$ in the random-field case [Fig. 1(b)] has fluctuations that scale like $Z^{1/2}$, it leads to the same random forces as the random-field potential [Fig. 1(a)] that shows order-one fluctuations. Therefore, we restrict analytical analysis to the case of random-field impurities. For Monte Carlo simulations we have used both types of disorder and found no significant difference. We will also assume that the disorder is weak, i.e., that the condition

$$\Gamma \gg \eta l \tag{3}$$

is fulfilled.

For $|\nabla Z|^2 \ll 1$, $g \approx 1$ and the equation of motion takes the form considered previously.[16,17,19,14] Below we summarize some of the results found in Refs. 19 and 14: Since the disorder is weak [see Eq. (3)], the interface is essentially flat on length scales $L \ll L_c$, where

$$L_c \approx l\left(\frac{\Gamma}{\eta l}\right)^{2/(4-D)} \gg l \tag{4}$$

is the so-called Larkin length. On larger scales the wall can adapt to the disorder and, as a result, it gets pinned for driving fields $h \lesssim h_p$ with

$$h_p \approx \Gamma l L_c^{-2} = \eta\left(\frac{\eta l}{\Gamma}\right)^{D/(4-D)} \ll \eta \tag{5}$$

for the pinning threshold. If h exceeds h_p, the wall starts to move. For $h \gg h_p$ the influence of the disorder is weak and the velocity is proportional to the driving field

$$v = \langle \dot{D} \rangle \approx \gamma h. \tag{6}$$

Corrections to this relation can be considered in the framework of high-velocity expansion, which can be expressed as a power series in

$$\frac{\xi_v}{L_c} \approx \left(\frac{h_p \gamma}{v}\right)^{1/(z-\zeta)}, \tag{7}$$

where ξ_v is dynamical correlation length that diverges as $v \to 0$; z and ζ are the dynamical and the roughness exponent, respectively. Outside the dynamical critical region, i.e., for $h - h_p \gg h_p$, $z=2$ and $\zeta=0$, respectively.

If the driving field h is so small that $\xi_v \gtrsim L_c$, the high-velocity expansion breaks down and a (functional) renormalization-group calculation has to be applied.[19] This leads to a renormalization of the mobility constant $\gamma \to \gamma_{\rm eff}$ with

$$\gamma_{\rm eff} \approx \gamma \left(\frac{\xi_v}{L_c}\right)^{(1/3)(4-D-\zeta)}. \tag{8}$$

After integrating out the interface fluctuations on the length scales $L \lesssim \xi_v$, the effective equation of motion for the interface profile $Z(\mathbf{x},t) = \langle Z(\mathbf{x},t)\rangle_{\xi_v, t_v}$ on large scales is given by

$$\frac{1}{\gamma_{\rm eff}} \frac{\partial Z}{\partial t} = \Gamma \nabla^2 Z + h - h_p + \eta_{\rm eff}(\mathbf{x}, v t). \tag{9}$$

Here $\langle\rangle_{\xi_v, t_v}$ denotes the spatial and time average over scales ξ_v and t_v, respectively, and $\eta_{\rm eff}$ is the renormalized random field that acts as a thermal noise. Since the latter leads to an interface roughness characterized by the exponent $\zeta_0 = (2-D)/2$, we may neglect the influence of the random field on these length scales. The mean velocity of the interface is given by

$$v \approx \gamma h_p \left(\frac{h - h_p}{h_p}\right)^{\theta}, \quad \frac{h-h_p}{h_p} \ll 1, \tag{10}$$

where $\theta = (z-\zeta)/(2-\zeta)$. z and ζ take now nontrivial values, which can be calculated by ϵ expansion in $D = 4 - \epsilon$ or determined numerically. For $D=1$ the ϵ expansion gives $\zeta = 1$ and $z = 4/3$ and hence $\theta = 1/3$, whereas the numerical values are $\zeta = 5/4$, $z \approx 1.42$, and $\theta \approx 1/4$.[20] To unify our results for the domain-wall velocity we rewrite Eqs. (6) and (10) as

$$v \approx h_p \gamma f\left(\frac{h}{h_p} - 1\right), \quad f(x) \approx \begin{cases} x^{\theta}, & x \ll 1 \\ x, & x \gg 1. \end{cases} \tag{11}$$

On the length scales $L_c \ll L \ll \xi_v$ the domain wall is rough,

$$w(L) = \langle [Z(\mathbf{x}_1) - Z(\mathbf{x}_2)]^2 \rangle^{1/2}_{|\mathbf{x}_1 - \mathbf{x}_2| = L} \approx l (L/L_c)^{\zeta}. \tag{12}$$

Bumps in the domain walls that emerge from random clusters heal on time scales

$$t_v \approx \frac{l}{v}\left(\frac{h_p}{v\lambda}\right)^{\zeta/(z-\zeta)} \approx \frac{l}{\gamma h_p}\left(\frac{h}{h_p} - 1\right)^{-z/(2-\zeta)}. \tag{13}$$

However, on larger scales $L \gg \xi_v$ the random field acts merely as a thermal noise and the roughness exponent is reduced to $\zeta = 1/2$ and $\zeta = 0$ (log) in $D=1$ and $D=2$ dimensions, respectively.

Thus, the moving domain wall heals its roughness at large distances $L > \xi_v$ and on the time scale $t > t_v$. This fact simplifies drastically theory of a domain wall moving with finite velocity in comparison to the theory of adiabatically moving domain walls and quasistatic hysteresis.[22,21] It allows one to consider domain wall on large distances as a smooth line, even as a straight line for homogeneous external field.

III. MOTION OF A RECTILINEAR DOMAIN WALL

We start with description of a rectilinear domain-wall motion. In the previous section we demonstrated that the domain-wall roughness can be ignored on a time scale $t > t_v$ and length scale $L > \xi_v$. Thus, locally the domain wall moves as a straight line. In some experiments only one domain wall survives (see Sec. VII). In this case the model problem of rectilinear domain-wall motion is close to reality. In other cases this problem is an important part of more complex problem describing either local properties of domain-wall motion or the order of magnitudes for the global motion. Thus, we consider the motion of a rectilinear domain wall under the action of magnetic field antiparallel to the magnetization.

We have mentioned already that the fluctuation bending of the domain wall can be neglected if the characteristic time of the process is much more than the bump healing time $t_v \propto v^{-z/(z-\zeta)}$. This requirement suggests that $\omega t_v \ll 1$. Anyway, this requirement must be satisfied since otherwise the average position of the domain wall almost does not change during half a period of oscillations.

The domain wall is assumed to be fixed at the left boundary of the sample $Z=0$ at the initial moment. We will solve equation of motion (6) for the domain-wall coordinate for harmonically oscillating magnetic field $h = h_0 \sin \omega t$. Instead of integrating it over time, we integrate it over field by the following change of coordinates:

$$dt = \frac{1}{\omega} \frac{dh}{\sqrt{h_0^2 - h^2}}. \tag{14}$$

After integration we find an expression for Z vs magnetic field h:

$$Z = \frac{\gamma}{\omega} \int_{h_p}^{h} f\left(\frac{h-h_p}{h_p}\right) \frac{dh}{\sqrt{h_0^2 - h^2}}. \tag{15}$$

This equation is correct for $h > h_p$. For smaller value of h the domain wall does not move: $Z = \text{const}$. Equation (15) should be complemented by a prescription to change the sign of the square root each time h reaches its maximum or minimum value $\pm h_0$ and by an initial condition $Z=0$ at $t=h=0$. The second necessary prescription is to substitute $h - h_p$ by $-h - h_p$ when h is negative. To transfer from the coordinate Z to the magnetic moment $\mathcal{M}$, the following representation is useful:

$$M = M_s \frac{2Z - L}{L}, \tag{16}$$

where M_s is the saturation magnetic moment. First of all we find two important boundary values for the amplitude h_0 that separate hysteresis loops of different shapes. The first of

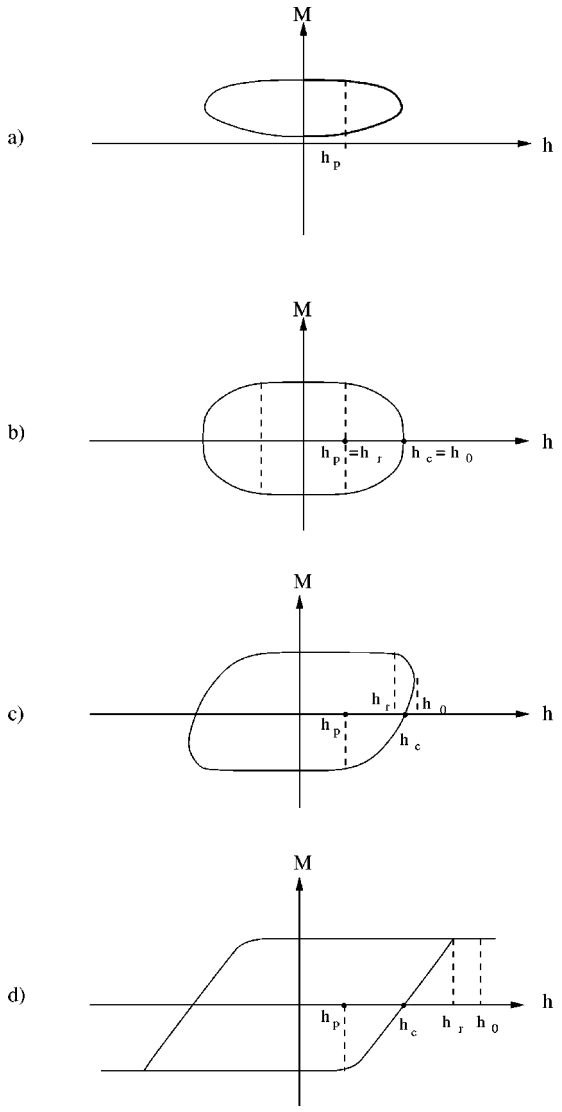

FIG. 2. Schematic pictures of hysteresis loops. (a) Incomplete HL for $h_0<h_{t1}$. (b) Symmetric HL for $h_0=h_{t1}$. (c) The HL for $h_{t1}<h_0<h_{t2}$. (d) The HL for $h_0>h_{t2}$. The values h_p, h_c, h_r, and h_0 are marked in all figures.

them is the dynamic threshold field h_{t1}, the smallest value of h_0 at which the domain walls reaches the right boundary of the sample $Z=L$. At $h_0<h_{t1}$ the magnetization is not reversed fully and the hysteresis loop is asymmetric [see Fig. 2(a)]. The hysteresis loop asymmetry was found earlier theoretically[4] and experimentally.[23] At larger values of h_0 the hysteresis loop is symmetric under inversion $h\rightarrow -h, M\rightarrow -M$ [Fig. 2(c)]. The value of h_{t1} is determined by the following equation:

$$\frac{\omega L}{2\gamma h_p}=\int_1^{h_{t1}/h_p} f(x-1)\frac{dx}{\sqrt{(h_{t1}/h_p)^2-x^2}}. \tag{17}$$

Note, that at $h_0=h_{t1}$ the hysteresis loop is symmetric with respect to reflections in the axis h and $\mathcal{M}$ [Fig. 2(b)]. From Eq. (17) it is seen that the ratio h_{t1}/h_p is the function of one dimensionless variable $\omega L/(\gamma h_p)$. This scaling relationship will be analyzed in detail later.

The next notorious field is h_{t2} defined as the value of h_0 at which the domain wall reaches the right end of the sample $Z=L$ during one fourth of period, just at $h=h_0$. The equation that defines h_{t2} is rather similar to that for h_{t1}:

$$\frac{\omega L}{\gamma h_p}=\int_1^{h_{t2}/h_p} f(x-1)\frac{dx}{\sqrt{(h_{t2}/h_p)^2-x^2}}. \tag{18}$$

It differs from Eq. (17) by the absence of a factor of 2 in the denominator of the left-hand side. The hysteresis loops corresponding to $h_0>h_{t2}$ acquire characteristic ''whiskers,'' single-valued pieces of the curve $M(h)$ that are absent in hysteresis curves for $h_0<h_{t2}$ [see Fig. 2(d)].

At a fixed $h_0>h_{t1}$ it is possible to define the coercive field h_c by the requirement $M(h_c)=0$. Finally, for $h_0>h_{t1}$ the so-called reversal field h_r can be defined as a value of the field h at which the magnetic moment reverses fully. At the value $h=h_r$ two branches of the hysteresis curve intersect each other. In other words, $Z(h_r)=L$. At h between h_r and h_0 the magnetic moment remains a constant $M=M_s$. The values h_c and h_r are shown in Fig. 2. Using Eqs. (15) and (16), we find

$$\frac{\omega L}{2\gamma h_p}=\int_{h_p}^{h_c} f\left(\frac{h-h_p}{h_p}\right)\frac{dh}{\sqrt{h_0^2-h^2}}. \tag{19}$$

Equation for h_r reads

$$\frac{\omega L}{\gamma h_p}=\int_{h_p}^{h_r} f\left(\frac{h-h_p}{h_p}\right)\frac{dh}{\sqrt{h_0^2-h^2}} \quad (h_0>h_{t2}), \tag{20}$$

$$\frac{\omega L}{\gamma h_p}=\left[\int_{h_p}^{h_r}+2\int_{h_r}^{h_0}\right] \times f\left(\frac{h-h_p}{h_p}\right)\frac{dh}{\sqrt{h_0^2-h^2}} \quad (h_{t1}<h_0<h_{t2}). \tag{21}$$

The ratios h_c/h_p and h_r/h_p are functions of two dimensionless variables $u=\omega L/(\gamma h_p)$ and $v=h_0/h_p$. Note that by knowledge of $w_2=h_{t2}/h_p$ (or $w_1=h_{t1}/h_p$) as a function of parameter $u=\omega L/\gamma h_p$ one can restore the function $f(x)$ solving the Abelian equation

$$f(x-1)=\frac{2}{\pi}\frac{d}{dx}\int_1^x \frac{u(w)w\,dw}{\sqrt{x^2-w^2}}. \tag{22}$$

The area of hysteresis loop $\mathcal{A}$ can be also expressed in the integral form

$$\mathcal{A}=4h_pM_s-4\frac{M_s}{L}\int_{h_p}^{h_r} Z(h)dh. \tag{23}$$

Now we proceed to the analysis of the hysteresis loop characteristics. It is controlled by parameters $u=\omega L/\gamma h_p$ and $v=h_0/h_p$. We start with small $u\ll 1$ imposing no restrictions on the value v. First we show that, at small u, the fields h_{t1} and h_{t2} are close to h_p. Indeed, it is clearly seen from Eqs. (17) and (18). Solving them approximately and employing the asymptotic formula for $f(x)$ at small x [Eq. (11)], we find

$$u/2=\frac{1}{\sqrt{2}}\int_1^{h_{t1}/h_p}(x-1)^{\theta}\frac{dx}{\sqrt{(h_{t1}/h_p)-x}}. \tag{24}$$

Introducing a new integration variable $s=(x-1)/(h_{t1}/h_p)-1$, Eq. (24) can be transformed as follows:

$$u/2=\frac{1}{\sqrt{2}}\left(\frac{h_{t1}}{h_p}-1\right)^{\theta+1/2}B(\theta+1,1/2), \tag{25}$$

where $B(x,y)$ is the Euler beta function. Using its standard representation,[24] one finds

$$\frac{h_{t1}}{h_p}-1\approx\left[\frac{(1+1/2\theta)\Gamma(\theta+1/2)}{\sqrt{2\pi}\Gamma(\theta)}u\right]^{2/(2\theta+1)}. \tag{26}$$

In a similar way the asymptotic of the field h_{t2} can be established. The ratio $(h_{t2}-h_p)/(h_{t1}-h_p)$ does not depend on the parameter u if u is small:

$$\frac{h_{t2}-h_p}{h_{t1}-h_p}=2^{2/(2\theta+1)}. \tag{27}$$

The shape of the hysteresis loop and its area depends not only on the parameter u, but also on the parameter $v=h_0/h_p$. If v is close to 1, i.e., if h_0 is also close to h_p, one can employ the low-field asymptotic of the function $f(x)$ [Eq. (11)] also in Eq. (20) for h_r. Then, for $h_0>h_{t2}$, the approximate equation for h_r reads

$$u=\frac{1}{\sqrt{2}}\int_1^{h_r/h_p}(x-1)^{\theta}\frac{dx}{\sqrt{v-x}}. \tag{28}$$

Introducing a new integration variable $s=(x-1)/(v-1)$, we find

$$u=(v-1)^{\theta+1/2}B(\theta+1,1/2;w);\quad w=\frac{h_r-h_p}{h_0-h_p}, \tag{29}$$

where $B(x,y;w)$ is incomplete B function, defined by an integral

$$B(x,y;w)=\int_0^w s^{x-1}(1-s)^{y-1}ds. \tag{30}$$

Thus, the ratio $w=(h_r-h_p)/(h_0-h_p)$ in this limit is a function of only one variable $u/(v-1)^{\theta+1/2}$. For h_0 close to h_{t2}, the field h_r is also close to h_p. If $u/(v-1)^{\theta+1/2}\ll 1$, the ratio w becomes small:

$$w\approx\left[\frac{\sqrt{2}u}{(\theta+1)(v-1)^{\theta+1/2}}\right]^{1/\theta+1}. \tag{31}$$

For completeness we present here equation for h_r in the range $h_{t1}<h_0<h_{t2}$ without derivation:

$$u=(v-1)^{\theta+1/2}[2B(\theta+1,1/2)-B(\theta+1,1/2;w)]. \tag{32}$$

If $u\ll 1$, but $v\gg 1$, the value h_r depends on the product uv. If it is small, then h_r is still close to h_p:

$$\frac{h_r-h_p}{h_p}=[(\theta+1)uv]^{1/(\theta+1)}=\left[\frac{(\theta+1)\omega h_0 L}{\gamma h_p^2}\right]^{1/(\theta+1)}. \tag{33}$$

In the opposite limiting case ($u\ll 1, uv\gg 1$) the field h_r is much larger than h_p, and the asymptotic $f(x)\sim x^{\theta}$ is not valid. In this case, the equation for h_r reads

$$h_r=\sqrt{\frac{\omega L}{\gamma}\left(2h_0-\frac{\omega L}{\gamma}\right)}. \tag{34}$$

Still, the reversal field h_r is much less than the amplitude h_0. For coercive field h_c in the range $u\ll 1, v\gg 1$ one finds

$$\frac{h_c}{h_p}-1=\left(\frac{h_r}{h_p}-1\right)2^{-1/(\theta+1)}\quad (uv\ll 1); \tag{35}$$

$$\frac{h_c}{h_p}\approx\frac{1}{\sqrt{2}}. \tag{36}$$

The shape and the area of the hysteresis loop depends on the same parameters $u=\omega L/(\gamma h_p)$ and $v=h_0/h_p$. We consider the range of small $u\ll 1$. If v is close to one, the low-field approximation for the function $f(x)$ may be used in Eq. (15) for z. Together with Eq. (16) it results in the following relation:

$$M=M_s\left[1-2\frac{B[\theta+1,1/2,(h-h_p)/(h_0-h_p)]}{B[\theta+1,1/2,(h_r-h_p)/(h_0-h_p)]}\right]. \tag{37}$$

For $-h_r<h<h_p$ on the lower branch of the hysteresis curve and for $-h_p<h<h_r$ on the upper branch $M=\pm M_s$. We presented here only a comparatively simple case $h_0>h_{t2}$. The case $h_0<h_{t2}$ is more complicated and we do not present here the explicit formulas for magnetization in this range of amplitudes.

For $u\ll 1$, $v\gg 1$, and $uv\ll 1$ we find in a similar way

$$M=M_s\left[1-2\left(\frac{h-h_p}{h_r-h_p}\right)^{\theta+1}\right]\quad (h_p<|h|<h_r). \tag{38}$$

and $M=M_s$ for $h_r<|h|<h_0$. Note that the hysteresis loop in this range of parameters is narrow, i.e., $h_r, h_c\ll h_0$.

In the interval $u\ll 1, uv\gg 1$ the value of h_r, according to Eq. (34), is much larger than h_p. One can neglect the threshold field and employ the linear asymptotic for $f(x)$ solving Eq. (15). The result is

$$Z(h)=\frac{\gamma}{\omega}(h_0-\sqrt{h_0^2-h^2}) \tag{39}$$

and

$$M=M_s\left[1-2\frac{\gamma}{\omega L}(h_0-\sqrt{h_0^2-h^2})\right]. \tag{40}$$

The latter two equations are valid in the interval of fields $|h|<h_r$. Beyond this interval the total magnetic moment is fixed at its saturation value. Note that a new characteristic length appears in the problem $L_\omega=\gamma h_0/\omega$. Below we present results for the hysteresis loop area $\mathcal{A}$ in the range of small u for different values of v without repeating of analogous calculations

(i) $v-1 \ll 1$:

$$\mathcal{A} \approx 4M_s h_p \times \left[1 + \frac{\sqrt{2}(v-1)^{\theta+1/2}}{u} \int_0^w B(\theta+1,1/2;x)dx \right]. \tag{41}$$

(ii) $v \gg 1, uv \ll 1$:

$$\mathcal{A} \approx 4M_s h_p \left[1 + \frac{[(\theta+1)uv]^{1/(\theta+1)}}{\theta+2} \right]. \tag{42}$$

(iii) $uv \gg 1$: In this case $h_r \gg h_p$.

Therefore all essential results formally coincide with those for $u \gg 1$ and the reader is referred to a corresponding subsection. Note that in the cases (i) and (ii) $\mathcal{A}$ is close to a constant value $\mathcal{A}_0 = 4M_s h_p$, but the deviation $\mathcal{A} - \mathcal{A}_0$ scales with two parameters u and v.

Now we proceed to a simpler case of large $u \gg 1$. In this case the dynamic threshold field h_{t1} is much larger than h_p:

$$h_{t1} = \frac{\omega L}{2\gamma}. \tag{43}$$

Therefore, one can neglect h_p when integrating Eq. (15) and others. Then we rediscover Eq. (39) for the coordinate. It implies that

$$h_{t2} = \frac{\omega L}{\gamma} = 2h_{t1}. \tag{44}$$

The equation for h_r coincides with Eq. (34). Coercive field h_c is determined by the equation

$$h_c = \sqrt{h_{t1}(2h_0 - h_{t1})}. \tag{45}$$

Equation (40) describes the shape of the hysteresis loop for $h_0 > h_{t2}$. It can be used also for the range of amplitudes $h_{t1} < h_0 < h_{t2}$ on the lower branch of the hysteresis curve $0 < h < h_0$. On the upper branch of this curve $h_r < h < h_0$ the sign of the square root must be reversed.

The hysteresis loop area is determined by the following equation:

$$\mathcal{A} \approx 4M_s h_r - \frac{2M_s h_r \gamma h_0}{\omega L} \times \left[2 - \frac{\arcsin(h_r/h_0)}{\sqrt{1-(h_r/h_0)^2}} - \sqrt{1-\left(\frac{h_r}{h_0}\right)^2} \right]. \tag{46}$$

This equation is valid for $h_0 > h_{t2}$. If, on the contrary, $h_0 < h_{t2}$, the area is

$$\mathcal{A} = 2M_s \int_0^{h_r} \left(1 - \frac{Z(h)}{L} \right) dh + 2M_s \int_{h_r}^{h_0} \frac{Z_+(h) - Z_-(h)}{L} dh, \tag{47}$$

where $Z_\pm(h)$ denote the value of coordinate on the upper $(+)$ and lower $(-)$ branches of the hysteresis curve, respectively. Performing the integration, we find

$$\mathcal{A} = 4M_s h_r \left(1 - \frac{\gamma h_0}{\omega L} \right) + \pi M_s h_0 \frac{\gamma h_0}{\omega L}. \tag{48}$$

One can observe that for the case $u \gg 1$ the static threshold field h_p does not enter physical results. Instead a new dimensionless parameter

$$u' = \omega L/(\gamma h_0) = L/L_\omega \tag{49}$$

emerges. In the range of existence of the full hysteresis loop $u' < 1/2$. Therefore u' cannot be large. However, it can be very small. It is worthwhile to consider separately the behavior of all values of interest in this asymptotic regime (large fields or small frequencies). For $u' \ll 1$ we find

$$h_r \approx h_c = h_0 \sqrt{u'}, \tag{50}$$

$$M(h) = M_s \left(1 - \frac{2}{u'} \frac{h^2}{h_0^2} \right), \tag{51}$$

$$\mathcal{A} \approx 4M_s h_r. \tag{52}$$

Near the threshold field h_{t1} the values of h_r and $\mathcal{A}$ are given by the following asymptotics:

$$h_r \approx 2\sqrt{h_{t1}(2h_0 - h_{t1})}, \tag{53}$$

$$\mathcal{A} = \frac{\pi M_s h_{t1}}{2} + 4\pi M_s \sqrt{h_{t1}(2h_0 - h_{t1})}. \tag{54}$$

Near the second threshold field h_{t2} the reversal field h_r is close to h_0:

$$h_r \approx h_0 - \frac{(h_0 - h_{t2})^2}{2h_{t2}}. \tag{55}$$

For $u' \ll 1$ we find scaling behavior of all hysteresis characteristics with universal critical exponents, independent of the pinning centers. Therefore, one can expect that the same scaling is valid for a clean ferromagnet with the relaxational dynamics. In particular, we have found that

$$\mathcal{A} \propto \omega^{1/2} h_0^{1/2}. \tag{56}$$

In this section we assumed that the magnetization in a single domain reaches its saturation value. If it is not the case, the magnetization on the parts of hysteresis curve beyond the hysteresis loop (''the whiskers'') is not a constant. The exact shape of the hysteresis curve in this case depends on the single-domain equilibrium magnetization curve.

IV. CREATION OF BUBBLES BY A MOVING DOMAIN WALL

In this section we show that, at sufficiently high magnetic field $h_p < h_0 < \eta$, the moving wall passes a series of defects that it cannot overcome. Instead it leaves closed domains of magnetization, opposite to the propagating magnetization, which serve as nuclei at the next half-cycle of the hysteresis process.

So far we assumed that an almost planar domain wall is pinned by typical fluctuations of the random field $\eta(\mathbf{r})$. In a (spherical) region of the volume $R^d, d=D+1$ a typical fluctuation of $\int_{R^d}\eta(\mathbf{r})d^dr$ is of the order $\pm\eta(l^dR^d)^{1/2}$, the corresponding probability is of the order 1/2. In the following we will consider the possibility of clusters of rare random-field fluctuations that may serve as nuclei of reversed spins when the field direction changes. A cluster of the size R consisting mainly of minimal negative value $-\eta$ of the random field has the probability $p(1,R)\simeq\exp[-(R/l)^D\ln 2]$. Such a cluster pins the domain wall for $h<\eta$ even if $h>h_p$. In general, if the concentration of $-\eta$ sites in a cluster is c, its probability $p(c,R)$ is of the order $\exp\{-(R/l)^d[c\ln c+(1-c)\ln(1-c)+\ln 2]\}$, and the pinning force density is of the order $(2c-1)\eta$. Since $h_p\ll\eta$, there is a field region $h_p<h<(2c-1)\eta$ in which the domain wall can be pinned locally by these rare fluctuations of the random field. The true pinning condition is now given by (see also Ref. 25 for similar considerations)

$$\frac{\Gamma}{R}+h-(2c-1)\eta<0, \tag{57}$$

where the first term denotes the Laplacian curvature force. Thus, the domain wall cannot overcome the pinning cluster if it has the size R bigger than $R_{\min}$, where

$$R_{\min}\approx\frac{\Gamma}{(2c-1)\eta-h}. \tag{58}$$

Using Eq. (58) we get

$$p(c,R_{\min})\approx\exp\left\{-\left[\frac{\Gamma}{(2c-1)\eta l-hl}\right]^d g(c)\right\}, \tag{59}$$

where

$$g(c)=c\ln c+(1-c)\ln(1-c)+\ln 2. \tag{60}$$

A closer inspection shows that in $d\geq 2$ dimensions $p(c,R_{\min})$ has its maximum at $c=1$. The mean distance between these strong pinning clusters is therefore of the order

$$L_{\text{cluster}}\approx l\exp\left\{\left[\frac{\Gamma}{(\eta-h_0)l}\right]^d\frac{\ln 2}{d}\right\}. \tag{61}$$

Here we have replaced h by by the maximum field strength during one cycle h_0. Since the interface cannot overcome the pinning cluster it will surround it and finally leave it behind as an island encircled by a domain wall (Fig. 3). These islands serve as nuclei of the favorite phase once the external field is reversed. Thus, in the expressions found in Sec. III the system size L has to be replaced by L_{cluster} as soon as $L>L_{\text{cluster}}$. If h_0 approaches and finally exceeds η, L_{cluster} diverges and hence this type of magnetization reversal process disappears. Domain walls originate then either from surfaces or from a nucleation process that we consider in the next section.

V. NUCLEATION-CONTROLLED HYSTERESIS

This mechanism works when the nucleation is the longest process. Let there exist a number of defects or impurities that lower the energy barrier for reversing magnetization locally.

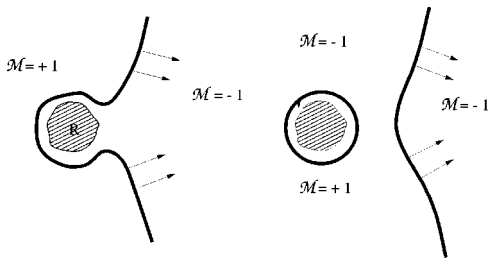

FIG. 3. Formation of a bubble by the moving domain wall.

Still, the reduced barrier Δ remains rather large so that the average reversal time $\tau_r(0)=\nu^{-1}\exp(\Delta/T)$ (ν is a microscopic frequency) is very large in comparison to the oscillation period: $\omega\tau_r\gg 1$. However, the reversal time depends on magnetic field

$$\tau_r(h)=\tau_r(0)\exp\left(-\frac{M_a h}{T}\right)=\nu^{-1}\exp\left(\frac{\Delta-M_a h}{T}\right), \tag{62}$$

where M_a is the saturation magnetic moment in the activation volume. We assume also that $\omega/\nu\ll 1$, but according to the accepted assumption $\exp(\Delta/T)\gg\nu/\omega$. Then the probability of spin reversal in an individual nucleus is negligibly small if $M_a h_0/T<\Delta/T-\ln[2\pi(\nu/\omega)]$. It becomes reasonably large starting from the dynamical threshold for the amplitude h_0:

$$h_{t1}=\frac{\Delta}{M_a}-\frac{T}{M_a}\ln\left(2\pi\frac{\nu}{\omega}\right). \tag{63}$$

Due to the sharpness of the exponential function, the reversal time $\tau_r(h)$ fast becomes much smaller than the oscillation period $2\pi/\omega$ as soon as $h(t)$ overcomes the threshold values h_{t1}. With the precision of a small parameter $\nu/\omega\exp(-\Delta/T)$ the reversal proceeds at a fixed field $h=h_{t1}$, which simultaneously plays the role of coercive field h_c and the reversal field h_r (see Sec. III). With the same accuracy the reversal proceeds at a moment of time $t_r=\omega^{-1}\arcsin(h_{t1}/h_0)$. The hysteresis loop has a rectangular shape (see Fig. 2). With a little higher accuracy the transition proceeds at a value of the phase $\varphi=\omega t$ determined by

$$\frac{M_a h_c}{T}\sin\varphi=\frac{\Delta}{T}-\ln\left(\frac{2\pi\nu}{\omega}\varphi\right), \tag{64}$$

which results in a corrected value of the coercive field

$$h_c=h_r=h_{t1}-\frac{T}{M_a}\ln\left(\arcsin\frac{h_{t1}}{h_0}\right). \tag{65}$$

As soon as the magnetization reverses in an individual nucleus, its walls expand quickly and, for a much shorter time than t_r, the full magnetic moment reverses. The case in which the propagation of domain walls is the longest process has been considered earlier in Secs. III and IV. The HLA for a rectangular loop is simply

$$\mathcal{A}=4M_s h_c$$

$$\approx 4\frac{M_s}{M_a}\Delta\left[1-\frac{T}{\Delta}\ln\frac{2\pi\nu}{\omega}-\frac{T}{\Delta}\ln\left(\arcsin\frac{h_{t1}}{h_0}\right)\right]. \tag{66}$$

Since $M_a h_{t1} \ll \Delta$ the value $1-(T/\Delta)\ln 2\pi\nu/\omega \ll 1$. For $h_0 \gg h_{t1}$ the HLA reads

$$\mathcal{A}=\mathcal{A}_0\left[1-\frac{T}{\Delta}\ln\frac{2\pi\nu}{\omega}+\frac{T}{\Delta}\ln\frac{h_0}{h_{t1}}\right]. \tag{67}$$

Note that at fixed ω and varying h_0 we find

$$\mathcal{A}=\mathcal{A}_0(\omega)\left[1-\frac{T}{M_a h_{t1}}\ln\frac{h_0}{h_{t1}}\right] \tag{68}$$

and $T/(M_a h_{t1}) \gg T/\Delta$. This theoretical result can be compared with recent measurements by Chen and Erskine.[12] They have measured the HLA for a thin film of Fe/W(110) in a wide range of frequencies ω and amplitudes h_0. They concluded that $\mathcal{A}\sim h_0^{\alpha}\omega^{\beta}$ with small exponents $\alpha\sim 0.2$ and very small exponent $\beta\sim 0.03-0.09$. Both exponents depend on temperature. These conclusions are compatible with our result [Eq. (67)]. Indeed, at such small values of exponents it is impossible to distinguish between the logarithmic dependence and the exponential dependence with a small exponent. Our predictions $\alpha=T/M_a h_{t1}$ and $\beta=T/\Delta$ agree with the experimentally discovered linear temperature dependence of the exponent β. It would be worthwhile to measure the frequency dependence of the dynamical threshold field h_{t1}. The fact of the existence of such a threshold has been observed in the same experiment. It should be noted that the value $T/M_a h_{t1}$ is not so small in the experiment $\sim 1/4$. Therefore we expect that our theory is correct with an accuracy of 25% only. On the other hand, the statement that there exists the powerlike dependence of the HLA on h_0 is not proved convincingly by this experiment since the interval of variation for h_0 was too small (the amplitude changed about 10 times).

So far we considered Δ and M_a as fixed values. This is correct if only one type of defect mediates the nucleation. More realistically these values are random. Then the defects with the minimal ratio Δ/M_a initiate the magnetization reversal process.

According to Eq. (63) h_{t1} becomes zero at very small frequencies, $\omega \leqslant 2\pi\nu\exp(-\Delta/T)$. Our theory is not valid for such a small frequency, but it reflects correctly the narrowing of the HL. On the other hand, the transition is smeared over the interval of magnetic field $\Delta h\sim T/M_a$. It is small in comparison to h if $h_0 M_a \gg T$. At a smaller amplitude h_0 the reversal is possible, but fluctuations of magnetization grow rapidly and become of the order of magnetization itself. In principle, it is possible that the nucleation time is of the same order of magnitude as that of the time of domain-wall propagation. However, since the nucleation time depends quickly on parameters, a small change of the regime makes one of the two times much larger than another. Thus, presumably the nucleation-mediated hysteresis loop has the rectangular shape, whereas a curved shape indicates that the hysteresis is associated with the domain-wall propagation or with strong fluctuations of magnetization.

A reason for the rounding of the HL in the case of the nucleation-controlled hysteresis can be that the sample is split into a number of magnetically disconnected grains with different Δ and M_a in each grain. Then the shape of the hysteresis loop reflects the distribution function for the ratio Δ/M_a.

VI. THE ADIABATIC DYNAMICS

In the case of strong Ising anisotropy the dynamic equation for magnetization m in the continuum limit has the form

$$\frac{\partial m}{\partial t}=-\Gamma\frac{\partial F}{\partial m}, \tag{69}$$

where F is a free energy. In the adiabatic limit the total magnetization $m(t)$ at the moment t can be represented as

$$m(t)=m_0[T,h(t)]+m_1(t), \tag{70}$$

where $m_0[T,h(t)]$ is the equilibrium value of magnetization for a given momentarly value of the magnetic field $h(t)$ and $m_1(t)$ is the deviation of magnetization from its equilibrium value. We discuss later restrictions imposed by the adiabaticity condition. Substituting $m(t)$ into Eq. (69), one finds an equation for m_1:

$$\chi\dot{h}=-\Gamma\frac{\partial^2 F}{\partial m^2}m_1, \tag{71}$$

where $\chi=\partial m/\partial h$ is the magnetic susceptibility. Equation (71) can be rewritten in a form

$$m_1=-\frac{\chi^2}{\Gamma}\dot{h}. \tag{72}$$

The hysteresis appears since the derivative $\dot{h}$ changes its sign when h passes its extremal values $\pm h_0$. For harmonically oscillating field $h(t)=h_0\sin\omega t$, its derivative may be expressed in terms of the field itself:

$$\dot{h}=\pm\omega\sqrt{h_0^2-h_c^2}. \tag{73}$$

Plugging Eq. (73) into Eq. (72), we find

$$m_1=\mp\frac{\omega\chi^2}{\Gamma}\sqrt{h_0^2-h^2}. \tag{74}$$

Perturbation theory is valid if $m_1 \ll (m_0)_{\max}=m_0(T,h_0)$, i.e., if $\omega\chi(h_0)/\Gamma \ll 1$. The coercive magnetic field h_c satisfies the following equation:

$$m_0(T,h_c)=|m_1(h_0,h_c,T)|=\frac{\omega\chi^2}{\Gamma}\sqrt{h_0^2-h_c^2}. \tag{75}$$

Assuming $h_c \ll h_0$, Eq. (75) can be transformed as follows:

$$m_0(T,h_c)=\frac{\omega\chi^2 h_0}{\Gamma}. \tag{76}$$

The HLA $\mathcal{A}$ can be calculated by knowledge of m_1:

$$\mathcal{A}=4\int_0^{h_0}m_1 dh=4\omega\int_0^{h_0}\frac{\chi^2}{\Gamma}\sqrt{h_0^2-h^2}dh. \tag{77}$$

Near the Curie point the relaxation time $\tau_c\propto\Gamma^{-1}\chi$ grows as $\tau_c\sim\tau_0\epsilon^{-\nu z}$, where $\epsilon=(T-T_c)/T_c$, ν is the correlation-length critical exponent ($\nu=1$ for the 2D Ising model), and z

is the dynamical critical exponent. The best numerical value for z is $z=2.17$ (for a modern review, see Ref. 26, and references therein). If $\epsilon=0$ and $h\neq 0$, the relaxation time is proportional to $h^{8z/15}$. For adiabaticity it is necessary that $\omega \ll \omega_c = \max[\tau_0^{-1}\epsilon^{z}, \tau_0^{-1}(h_0/h_{\rm ex})^{8z/15}]$, where $h_{\rm ex}$ is the saturation (exchange) field.

The amplitude h_0 should be considered as small [case (i)] or large [case (ii)] depending on its ratio to a characteristic field $h^*(\epsilon)=h_{ex}\epsilon^{15/8}$. For a small amplitude $h_0 \ll h^*(\epsilon)$ one can employ a linear approximation for $m_0(T,h)=\chi(\epsilon)h$ to solve Eq. (76). Then $h_c = h_0\omega\chi(\epsilon)/\Gamma(\epsilon)$. Next we use the relation $\chi(\epsilon)/\Gamma \sim \tau_0\epsilon^{-z}$ to find

$$h_c = \omega h_0 \tau_0 \epsilon^{-z} = \omega h_0 \tau_0 \epsilon^{-2.17}. \tag{78}$$

For a large amplitude $h_0 \gg h^*(\epsilon)$ a dimensionless ratio $\kappa = \omega\chi(\epsilon)/\Gamma(\epsilon)$ matters. If it is much less than the large value h_0/h^*, then the coercive force can be calculated as $h_c = \kappa h_0$, exactly as in Eq. (78). Otherwise $h_c \gg h^*$. Then an approximate solution of Eq. (76) reads

$$h_c \approx h_{\rm ex}\left(\omega\tau_0\frac{h_0}{h_{\rm ex}}\right)^{-15/(15+8z)} \sim h_{\rm ex}\left(\omega\tau_0\frac{h_0}{h_{\rm ex}}\right)^{-0.46}. \tag{79}$$

Corresponding results for the HLA are as follows:

$$\text{(i)} \quad \mathcal{A} \propto \omega h_0^2 \frac{\chi^2(\epsilon)}{\Gamma(\epsilon)} \sim \omega h_0^2 \tau_0 \epsilon^{-z-\gamma} \sim \omega h_0^2 \tau_0 \epsilon^{-3.92}, \tag{80}$$

$$\text{(ii)} \quad \mathcal{A} \propto \omega h_0 \frac{h^*(\epsilon)\chi^2(\epsilon)}{\Gamma(\epsilon)} = \omega h_0 h_{ex} \tau_0 \epsilon^{-2.04}. \tag{81}$$

Though we cannot calculate explicitly the hysteresis loop area in the opposite, antiadiabatic regime $\omega_c \ll \omega \ll J/\hbar$, the dimensionality arguments lead to a necessary estimate. Indeed, according to the general equation (77), its scaling dimensionality is

$$\mathcal{A} \propto \chi h_0^2, \tag{82}$$

where we have used the facts that ω and Γ/χ have the same dimensionality and that $h_0 \ll h^*(\omega) = h_{ex}(\hbar\omega/J)^{8z/15}$. Thus,

$$\mathcal{A} \propto \chi(\omega) h_0^2 \propto \omega^{-\gamma/z} h_0^2 = \omega^{-0.8} h_0^2. \tag{83}$$

Typical orders of magnitude are $\tau_0^{-1} \sim J/\hbar \sim 4\times 10^{13}$ Hz; $\epsilon \sim 10^{-3}$; $\omega_c(\epsilon) \sim 2$ MHz; $h^*(\epsilon) \sim 3$ Oe; $T_c \sim 300$ K; $T - T_c \sim 0.3$ K.

Note that all calculations in this section have been made for $T > T_c$, so that we could ignore the problem of nucleation and domain-wall motion. Below the Curie temperature the problem of spinodal decomposition appears when the field reaches the spinodal. Then, again, either the nucleation or the domain-wall motion prevails in the magnetization reversal. It does not happen if either $h_0 \gg h^*(\epsilon)$ or $\omega \gg \tau_c^{-1}$. Then one can use previous results. However, if these conditions are not met, then either nucleation or the domain wall propagation prevails in the magnetization reversal process. To establish what is more important, let us consider corresponding time scales. The nucleation time for a pure sample is

$$\tau_r = \tau_c(\epsilon)\exp\left(\frac{h^*(\epsilon)}{h}\right). \tag{84}$$

Though this time scale grows at approaching to the Curie temperature, it can be sufficiently small. Its minimization over ϵ at fixed value of h gives

$$\tau_r \propto \tau_0\left(\frac{h_{ex}}{h}\right)^{z/(\beta+\gamma)} = \tau_0\left(\frac{h_{ex}}{h}\right)^{1.157}. \tag{85}$$

For the exchange field of about 10^6 Oe and external field of about 100 Oe the nucleation time becomes of the order of 10^{-9} sec. Thus, the nucleation proceeds very fast and the process of domain-wall propagation prevails in this range of fields and frequencies. This conclusion explains the results of our numerical calculations for temperatures close to the Curie point (see Sec. VII).

VII. SIMULATION OF THE DOMAIN GROWTH

In this section the process of magnetization reversal in a few-monolayers-thick magnetic film is modeled by an analogous process in the two-dimensional Ising model with the Glauber dynamics. In simulation we neglect the dipole-dipole interaction and demagnetization effects. The Hamiltonian of the Ising system in a time-dependent field $h(t)$ has a form

$$\mathcal{H}_b = -\frac{1}{2}\sum_{\mathbf{r},a} J_{\mathbf{a}}(\mathbf{r})\sigma_{\mathbf{r}}\sigma_{\mathbf{r}+\mathbf{a}} - h(t)\sum_{\mathbf{r}} \sigma_{\mathbf{r}}, \tag{86}$$

where summation over $\mathbf{r}$ runs over the lattice sites and $\mathbf{a}$ labels nearest neighbors. In a perfect ferromagnetic film, $J_{\mathbf{a}}(\mathbf{r}) = J_0 > 0$ independently on $\mathbf{r}$. In the case of quenched disorder we assume that the exchange integral is ferromagnetic $[J_{\mathbf{a}}(\mathbf{r}) = J_0 > 0]$ with the probability $1-\vartheta$ and antiferromagnetic $[J_{\mathbf{a}}(\mathbf{r}) = -J_0 < 0]$ with the probability ϑ ($\vartheta \ll 1$). No correlation in the location of random bonds is assumed. In Sec. II it is shown that this type of disorder is of general importance for the problem of the domain wall moving in the disordered media. Weak random-bond disorder does not destroy the long-range order in the 2D Ising model. The magnetic field $h(t)$ is supposed to oscillate harmonically as $h(t) = h_0\sin(\omega t)$, unless a different assumption is not specially formulated. The process of magnetization reversal can be divided into two stages: nucleation of domains with opposite magnetization and growth of these domains. Which process dominates depends on system parameters and their history. In this section we consider a limit of the nucleation time much smaller than the growth time. Then the magnetization reversal process is dominated by the domain-wall propagation discussed in Secs. II and III.

We employed the Monte Carlo simulation with the Glauber dynamics (see, e.g., Ref. 27) to check Eq. (6) for perfect systems and systems with disorder. We modeled the disorder by a small concentration of randomly distributed antiferromagnetic bonds. This disorder weakly influences the phase diagram and results only in a small shift of T_c, where T_c is an Ising transition temperature of the model equation (86) with $h=0$. We have found the linear dependence of domain-wall velocity on applied magnetic field at all relevant temperatures with and without disorder. Apparently, in

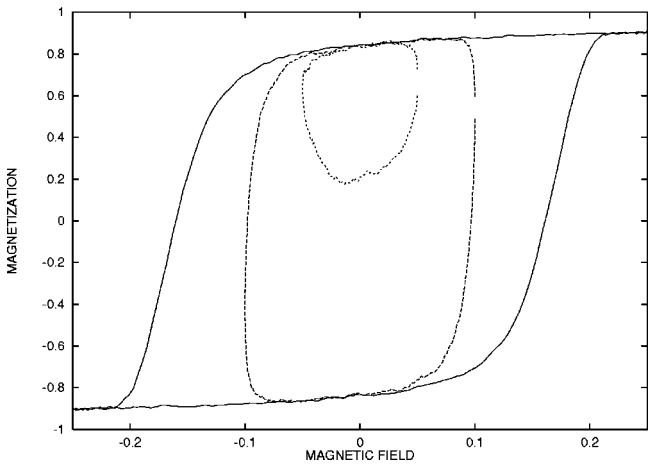

FIG. 4. Simulated hysteresis loops for different values of h_0 and constant ω. The observed hysteresis-loop behavior obeys the general classification scheme developed in Secs. II and III and shown in Fig. 2 (see explanation in text).

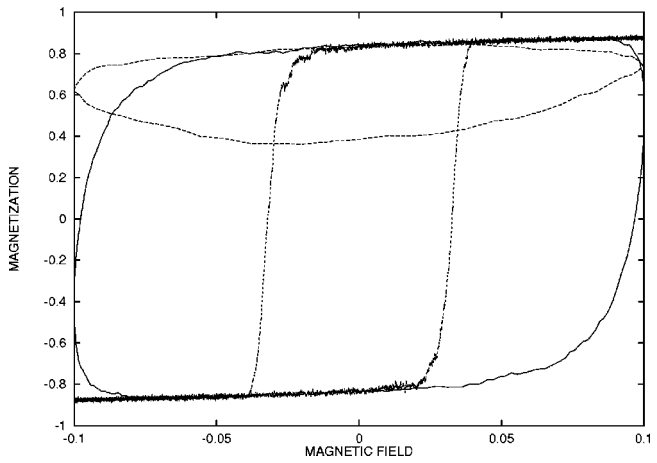

FIG. 5. Simulated hysteresis loops for different values of ω and constant h_0. The observed hysteresis-loop behavior obeys the general classification scheme developed in Secs. II and III and shown in Fig. 2 (see explanation in text).

these simulations we dealt with the limit of weak pinning, so that $h_p \ll h_0$. However, at low temperatures ($T < 0.1T_c$) even a small disorder, which almost does not change the thermodynamics, modifies the domain-wall dynamics drastically. The results related to the domain-wall motion and hysteresis phenomena in a weakly disordered system at low temperature will be discussed elsewhere.

The domain growth was studied in two geometries: stripes and circles. To distinguish the domain growth from domain nucleation we examined either a specially prepared defect for fast nucleation or a prepared nucleus with the opposite direction of magnetization possessing the shape of the circle or stripe. In both cases the magnetization changed in accordance with the model of a straight DW, i.e., it was similar to Eq. (40).

Simulated hysteresis loops for different values of magnetic-field amplitudes ($h_0 = 0.025J$, $h_0 = 0.05J$, and $h_0 = 0.125J$) and constant period of 8×10^3 Monte Carlo steps are shown in Fig. 4. Hysteresis loops for different periods (4×10^3, 8×10^3, and 256×10^3 Monte Carlo steps) and constant $h_0 = 0.05J$ are shown in Fig. 5. The observed hysteresis-loop behavior obeys the general classification scheme developed in Secs. II and III (compare with Fig. 2). In particular, the asymmetric loops in Figs. 4 and 5 correspond to the loop in Fig. 2(a), the loops with whiskers in Figs. 4 and 5 correspond to the loop in Fig. 2(d), and the symmetric loops without whiskers in Figs. 4 and 5 correspond to the loop in Fig. 2(c). The concentration of random bonds in the system was $\approx 0.8\%$.

Figure 6 shows the time sequence of inflating domains for the system with $T = 0.5T_c$ and $h_0 = 0.25J$. The concentration of random bonds in this case was $\approx 3\%$. The nucleation first proceeds at three regions, then the corresponding domains inflate rapidly and two of them merge. The time development of the inflation process is shown in Fig. 6. The total magnetization for each snapshot is indicated in Fig. 6. The analysis shows that the inflation of a domain with reversed magnetization is described by simple law [Eq. (40)].

Let L_N be the mean distance between nucleation centers. It plays the same role as the system size L in Sec. III. The ratio $L_N/L_\omega = u_N$ is an analog of the dimensionless parameter u' introduced by Eq. (49). In the limit $L_N \ll L_\omega$ (compare Sec. III) the domain growth will be fast enough to provide the full hysteresis cycle with $h_r \ll h_0$ [see Fig. 2(d)]. We evaluated the scaling behavior of h_c and $\mathcal{A}$ as a function of ω and h_0 in the limit $L_N \ll L_\omega$ using Eq. (39). To deal with the domain-wall propagation-dominated hysteresis, we considered temperature close to the Curie point. We argued earlier (see Sec. VI) that in this case the nucleation proceeds fast enough. Figure 7 shows domain distribution in the applied reversed magnetic field at $T = 0.95T_c$. Multiple nuclei that are seen in this picture serve as evidence that the nucleation is really fast enough.

At $h = h_c$ the typical domain size L_d is of the order of the mean distance between domains. Since $L_N \ll L_\omega$, we conclude that $h_c \ll h_0$, and $L_N \approx (\gamma/h_0\omega)(h_c)^2$. Assuming that the average distance between nucleation centers does not depend significantly on ω, we immediately obtain that the coercive field h_c scales as $h_c \propto \sqrt{\omega}$ [compare with Eq. (50)]. If, in addition, the average distance between nucleation centers does not depend significantly on h_0, we have $h_c \propto \sqrt{h_0\omega}$. If we assume that the magnetic field is strong enough and saturation magnetization does not change significantly by changing h_0, the HLA area scales in the same way as h_c, i.e., $\mathcal{A} \propto \sqrt{h_0\omega}$. This is a simplified qualitative version of arguments leading to Eq. (56) of Sec. III.

Figure 8 shows the dependence of the hysteresis loop area $\mathcal{A}$ on ω in the double logarithmic coordinates at $T = T_c$. The $\sqrt{\omega}$ scaling behavior is valid over three decades of the ω variation. However, the range of magnetic-field values available is only one decade. For this reason we have only checked that magnetic-field dependence is consistent with $\mathcal{A} \propto \sqrt{h_0}$ dependence.

To check the proposed mechanism of magnetization reversal we have also simulated this process for the magnetic field $h = h_0 \sin^3(\omega t)$. In this case both h_c and $\mathcal{A}$ scale in accordance with the analytical results as $\omega^{3/4}$.

Though we put $T = T_c$, the system is far away from the critical point due to a relatively large magnetic field. Indeed, one can estimate ϵ defined in Sec. VI from the relation $\epsilon \approx (h_0/h_{ex})^{8/15}$ (see Sec. VI). In our simulations h_0/h_{ex}

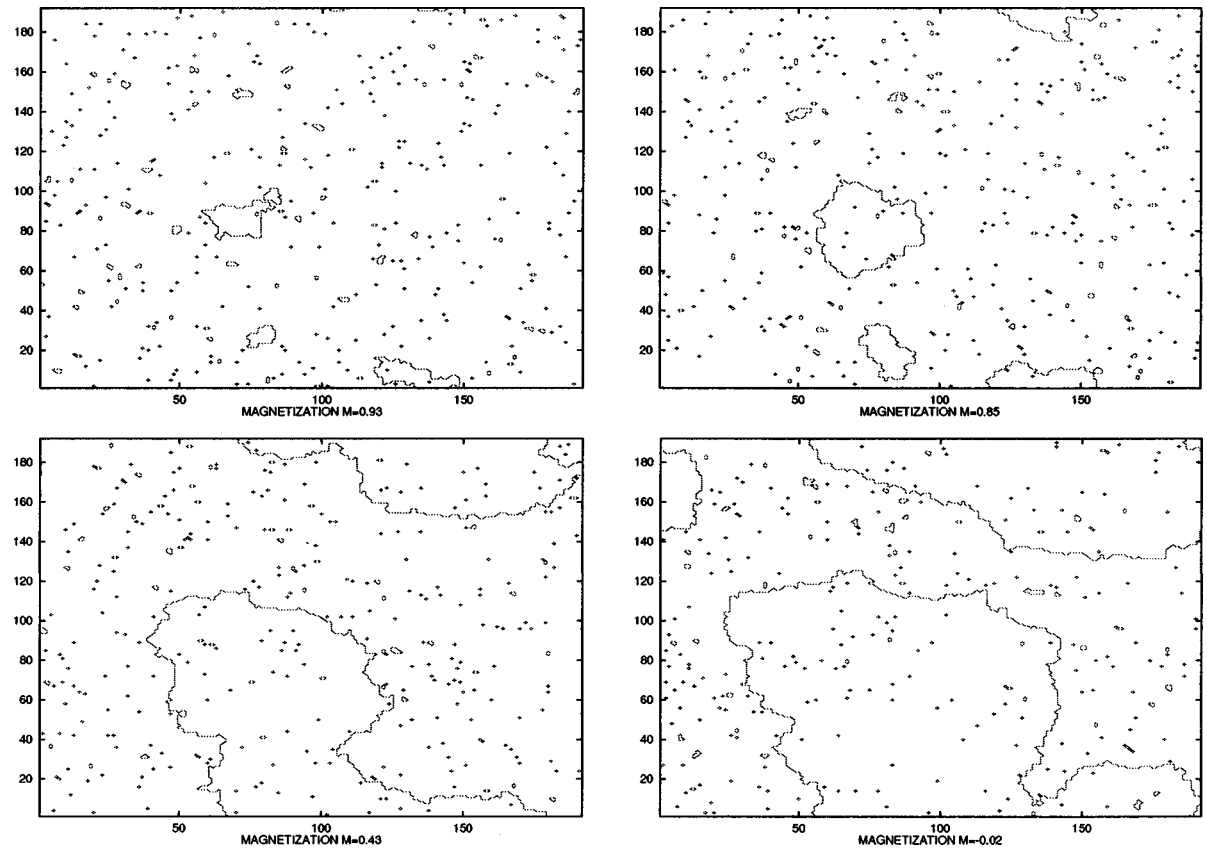

FIG. 6. Inflation of domains with opposite magnetization in an Ising model in reversed magnetic field with $h_0=0.25J$ at $T=0.5T_c$ for the system of the size 192×192 with periodic boundary conditions and with random frozen defects (antiferromagnetic bonds) with concentration 0.03. Each dot corresponds to the bond with opposite spin orientation.

$=0.05$–0.005, which gives $\epsilon\approx0.2$–0.06. It means that the deviation from the critical point is large enough. With these values of fields, our system is also far away from the strong fluctuation regime described in Sec. VI. A necessary condition for this regime is that $m_0\ll1$. The magnetic moment m_0 scales as $m_0\propto(h/h_{\rm ex})^{1/15}$. Therefore the field $h_0\approx0.005h_{\rm ex}$ is rather strong; it gives $m_0\approx0.7$.

With the temperature decreasing, away from critical region the HLA deviates strongly from the power-law behavior as it follows from Fig. 8. We expect that the HL changes its shape and characteristics from those dominated by domain-wall propagation to those dominated by nucleation. The crossover behavior cannot be described by a single power law.

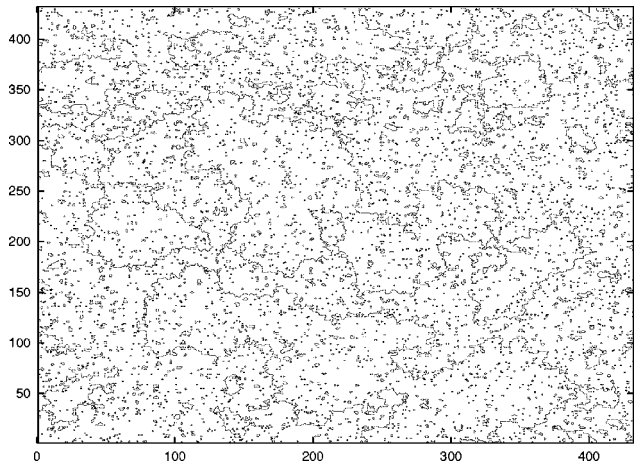

FIG. 7. Domain-wall distribution in an Ising model in reversed magnetic field with $h_0=0.05J$ at $T=0.95T_c$ for the system of the size 432×432 with periodic boundary conditions. Each dot corresponds to the bond with opposite spin orientation.

VIII. CONCLUSIONS

We studied the main mechanisms of the hysteresis in a ferromagnet: the driven DW motion, nucleation and retarda-

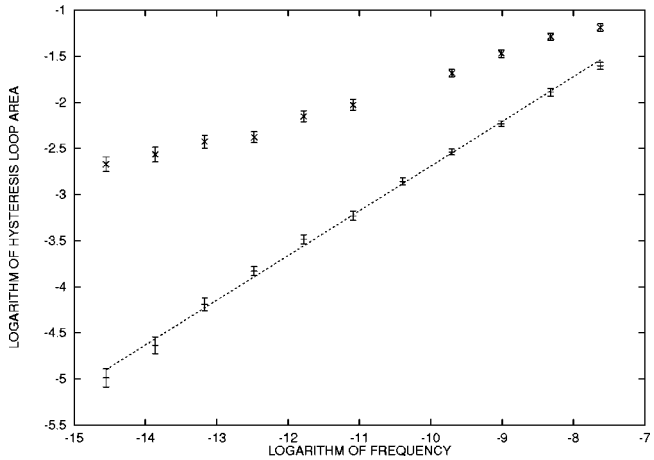

FIG. 8. Hysteresis-loop area as a function of frequency in double logarithmic coordinates for the magnetic field with amplitude $h_0=0.05J$ at $T=T_c$ (lower line) and at $T=0.95T_c$.

tion in nonlinear magnetization dynamics. Each of them may be dominant at proper conditions. A process is dominant if it provides maximum value for the coercive field h_c.

In the background of the general theory of the interface motion in a random medium we studied the hysteresis process controlled by the DW motion. We introduced two dynamic threshold fields h_{t1} and h_{t2} corresponding to the occurrence of the full magnetization reversal and to the occurrence of the single-valued parts on the hysteresis curve, respectively. These dynamical threshold fields are larger than the static threshold field h_p which is required to start a motion of the DW. We established that h_{t1} and h_{t2} measured in units h_p are functions of one dimensionless parameter $u = \omega L/\gamma h_p$ (see notations in Secs. I, II, and III). The coercive field h_c and the reversal field h_r, measured in the same units, can be expressed in terms of one function of two dimensionless parameters:

$$h_c = h_p F\left(\frac{\omega L}{2\gamma h_p}, \frac{h_0}{h_p}\right); \quad h_r = h_p F\left(\frac{\omega L}{\gamma h_p}, \frac{h_0}{h_p}\right). \tag{87}$$

Experimental observation of this type of scaling would be the best indirect evidence of the DW motion-controlled hysteresis. The direct observation of the DW motion by scanning magneto-optical Kerr effect and scanning tunneling microscope methods in principle is possible[28] and is much appreciated. At large fields $h_0 \gg h_p$ the defects are inessential. Therefore, the dependence on h_p must vanish from scaling laws (87). It happens indeed, and both fields h_c and h_r are expressed in terms of one dimensionless parameter:

$$h_c = h_0 F\left(\frac{\omega L}{2\gamma h_0}\right); \quad h_r = h_0 F\left(\frac{\omega L}{\gamma h_0}\right), \tag{88}$$

where $F(x) = 2\sqrt{x(1-x)}$. Note that in this limit the value h_p vanishes from equations for the dynamic threshold fields as well: $h_{t1} = \omega L/\gamma$, $h_{t2} = 2h_{t1}$. We presented also corresponding equations for the HLA on which the most experimental efforts were concentrated. However, we would like to emphasize that the HLA is not the only measurable characteristics of the HL and even not the most informative its characteristics: the fields h_{t1}, h_{t2}, h_c, and h_r, as well as the shape of the hysteresis curve, are not less interesting. The functional dependence of the fields h_{t1} and h_{t2} on h_0 at h_0 not much overcoming the static threshold field h_p allows one to restore the basic function $f((h-h_p)/h_p)$ of the theory of the DW motion in a defect medium.

For sufficiently large h_0 the length L in Eqs. (87) and (88) and others is the size of the system. Thus, the size effect is observable in the HL characteristics. However, at fields larger than h_p, but still smaller than the maximum defect strength, the moving DW produces bubbles playing the role of ready nuclei for magnetization reversal at the next half-cycle of the hysteresis loop. Thus, the length L in this case is the average distance between the bubbles. Its strong dependence on the field amplitude h_0 makes the scaling laws (87) and (88) less transparent, but they become size independent. The scaling becomes simple again if the dominant defects are of topographic origin. The density of topographic defects is independent on the amplitude of magnetic field. Then L is the average distance between such defects.

In the case, when the driven DW's are almost free ($h_0 \gg h_p$) and the HL is narrow ($h_0 \gg h_{t1}$), the HLA was found to be proportional to $\omega^{1/2} h_0^{1/2}$. This conclusion is supported by our numerical Monte Carlo simulation.

In the nucleation-controlled process almost rectangular HL shape is expected, unless the sample is divided into a multitude of magnetically disconnected grains. Note that the shape of almost vertical parts of the HL in this case is determined by the DW motion and, therefore, is universal. In the case of nucleation-controlled hysteresis the HLA must grow logarithmically with the frequency and amplitude of magnetic field. However, the coefficient at the logarithm of frequency is smaller than that at the logarithm of the amplitude. Slow nonlinear critical dynamics may produce the HL with various scaling limits as described in Sec. VI.

The comparison with the experiment is still rather poor since there is no systematic study of the HL characteristics as functions of dimensionless parameters. The experimental efforts were focused on the HLA, but the precision of the measurements is not high enough for reliable determination of scaling. Suen and Erskine[9] reported the observation of linear dependence of the HLA on the logarithm of frequency[33] with the coefficient proportional to temperature. Both these facts agree with our theory. However, they also claimed the power dependence of the HLA on the amplitude h_0 with the exponent about 1/4. This dependence contradicts our theory. The reason for discrepancy is not yet clear. The interval of variation of h_0 is not large enough to establish the exponential dependence reliably, but it definitely deviates from logarithm. On the other hand, our theory gives logarithmic dependence on h_0 only if $h_0 \gg h_{t1}$. Further studies both theoretical and experimental are necessary to clarify the situation.

Our numerical simulations show visibly the formation and propagation of domain walls as the dominant process at high temperature. The domain walls look rather rough. It can happen as a consequence of strong critical fluctuations that are not taken into account in our DW motion theory, or it may follow from the fact that the dimensionality 2 is the marginal for the development of roughness due to defects (the roughness exponent ζ is equal to 1 for $d=2$). Nevertheless, the scaling low $\mathcal{A} \propto \omega^{1/2} h_0^{1/2}$ for $h \gg h_p$ is confirmed in numerical simulations at high temperatures. At lower temperature the nucleation becomes dominant.

An interesting possibility to verify our predictions for the domain-growth-controlled hysteresis is a study of a hysteresis of adsorption isotherms close to equilibrium conditions. The process of close to equilibrium adsorption can be studied experimentally for noble gases (see, e.g., Ref. 29). The quasiequilibrium desorption of helium films has been studied in Ref. 30. In the case of equilibrium adsorption the chemical potential plays the role of magnetic field and the coverage plays the role of magnetization. The domain-wall width for adsorbed systems is only one lattice period wide. For this reason one can expect rather small nucleation barriers for equilibrium adsorption and a broader range of existence for domain-growth-controlled hysteresis than in magnetic films. More detailed analysis is given in Ref. 31. Though the adsorption isotherms have been measured starting from Langmuir, no hysteresis-loop measurements have been performed

until recently. The first such experiment by H. Pfnür and K. Budde[32] gave values of β close to 1/2.

ACKNOWLEDGMENTS

This work was partly supported by the DOE, Grant No. DE-FG03-96ER 45598 and by the NSF, Grant No. DMR-97-05182. T.N. acknowledges the support of the German-Israeli Foundation (GIF) and the Volkswagen Foundation and is grateful for the hospitality of the ENS Paris, where part of this work was done. We thank J. Erskine for interesting and fruitful discussions, and H. Pfnür for sending us the experimental results (Ref. 32) prior to publication. One of the authors (V.P.) is grateful to the Sonderforschungsbereich 341 for supporting him during his stay at Cologne University, where this work has been completed. He also thanks Professor J. Zittartz for the hospitality extended to him at Cologne.

*Also at Institute of Physics, 252028 Kiev, Ukraine.

[1] C.P. Steinmetz, Trans. Am. Inst. Electr. Eng. **9**, 3 (1892).

[2] W.S. Lo and R. Pelcovits, Phys. Rev. A **42**, 7471 (1990).

[3] D. Dhar and P.B. Thomas, J. Phys. A **25**, 4967 (1992).

[4] M. Acharyya and B.K. Chakrabarti, Physica A **192**, 471 (1993); Phys. Rev. B **52**, 6550 (1995).

[5] C.N. Luse and A. Zangwill, Phys. Rev. E **50**, 224 (1994).

[6] M. Rao, H. R. Krishnamurthy, and R. Pandit, J. Phys. C **1**, 9061 (1989); M. Rao, H. R. Krishnamurthy, and R. Pandit, Phys. Rev. B **42**, 856 (1990); J. Appl. Phys. **67**, 5451 (1990); M. Rao and R. Pandit, Phys. Rev. B **43**, 3373 (1991); M. Rao, *ibid.* **45**, 7529 (1992); S. Sengupta, Y. J. Marathe, and S. Puri, *ibid.* **45**, 7828 (1992).

[7] Y.L. He and G.C. Wang, Phys. Rev. Lett. **70**, 2336 (1993).

[8] Q. Jiang, H.-N. Yang, and G.C. Wang, Phys. Rev. B **52**, 14 911 (1995).

[9] J.-S. Suen and J.L. Erskine, Phys. Rev. Lett. **78**, 3567 (1997).

[10] P. Bruno, G. Bayreuther, P. Beauvillain, C. Chappert, G. Lugert, D. Renard, J.P. Renard, and J. Seiden, J. Appl. Phys. **68**, 5759 (1990).

[11] B. Raquet, R. Mamy, and J.C. Ousset, Phys. Rev. B **54**, 4128 (1996).

[12] J. Chen and J. L. Erskine, Phys. Rev. Lett. **68**, 1212 (1992).

[13] W. Weber, C. H. Back, A. Bischof, D. Pescia, and R. Allenspach, Nature (London) **376**, 788 (1995).

[14] O. Narayan and D. S. Fisher, Phys. Rev. B **48**, 7030 (1993).

[15] R. Bausch, V. Dohm, H. K. Janssen, and R. K. P. Zia, Phys. Rev. Lett. **47**, 1837 (1981).

[16] M. V. Feigel'man, Zh. Éksp. Teor. Fiz. **85**, 1851 (1983) [Sov. Phys. JETP **58**, 1076 (1983)].

[17] J. Koplik and H. Levine, Phys. Rev. B **32**, 280 (1985).

[18] T. Nattermann, Z. Phys. B **54**, 247 (1984).

[19] T. Nattermann, S. Stepanow, L.-H. Tang, and H. Leschhorn, J. Phys. II **2**, 1483 (1992).

[20] H. Leschhorn, Physica A **195**, 324 (1993).

[21] D. Dhar, P. Shukla, and J. P. Sethna, J. Phys. A **30**, 5259 (1997).

[22] J. P. Sethna, K. Dahmen, S. Kartha, J. A. Krumhansl, B. W. Roberts, and J. D. Shore, Phys. Rev. Lett. **70**, 3347 (1993).

[23] J. L. Erskine (private communication).

[24] I. S. Gradstein and I. M. Ryzik, *Table of Integrals, Series, and Products*, 5th ed. (Academic, Boston, 1994).

[25] A. Engel and W. Ebeling, Phys. Lett. A **122**, 20 (1987).

[26] J. Adler, in *Annual Reviews of Computational Physics IV*, edited by D. Stauffer (World Scientific, Singapore, 1996); M. P. Nightingale and H. W. Blöte, Phys. Rev. Lett. **76**, 4548 (1996).

[27] K. Binder and D. Stauffer, *Applications of the Monte-Carlo Method in Statistical Physics*, Topics in Current Physics Vol. 36 (Springer, Berlin, 1987).

[28] L. H. Bennett, R. D. McMichael, L. J. Swartzendruber, S. Hua, D. S. Lashmore, A. J. Shapiro, V. S. Gornakov, L. M. Dedukh, and V. I. Nikitenko, IEEE Trans. Magn. **31**, 4088 (1995).

[29] L. W. Bruch, M. W. Cole, and E. Zaremba, *Physical Adsorption: Forces and Phenomena* (Oxford University Press, Oxford, 1997).

[30] M. Weimer, R. M. Housley, and D. L. Goodstein, Phys. Rev. B **36**, 5199 (1987).

[31] I. F. Lyuksyutov, H. Pfnür, and H.-U. Everts, Europhys. Lett. **41**, 395 (1998).

[32] K. Budde, I. F. Lyuksyutov, H. Pfnür, G. Godzik, and H. U. Everts, cond-mat/9807225 (unpublished).

[33] Suen and Erskine claimed a power dependence with a small exponent, but in the framework of their data it is indistinguishable from the logarithm.